NASA TECHNICAL NOTE

NASA TN D-6576

ROTATIONAL-TEMPERATURE DETERMINATION IN FLOWING NITROGEN USING AN ELECTRON BEAM

by D. C. Lillicrap and L. P. Lee

Langley Research Center
Hampton, Va. 23365

NATIONAL AERONAUTICS AND SPACE ADMINISTRATION • WASHINGTON, D. C. • DECEMBER 1971

1. Report No.	2. Government Accession No.	3. Recipient's Catalog No.
NASA TN D-6576		

4. Title and Subtitle	5. Report Date
ROTATIONAL-TEMPERATURE DETERMINATION IN FLOWING NITROGEN USING AN ELECTRON BEAM	December 1971
	6. Performing Organization Code
7. Author(s)	8. Performing Organization Report No.
D. C. Lillicrap and Louise P. Lee	L-8011
	10. Work Unit No.
9. Performing Organization Name and Address	117-07-01-06
NASA Langley Research Center Hampton, Va. 23365	11. Contract or Grant No.
	13. Type of Report and Period Covered
12. Sponsoring Agency Name and Address	Technical Note
National Aeronautics and Space Administration Washington, D.C. 20546	14. Sponsoring Agency Code

15. Supplementary Notes

This research was accomplished while the first author was an NRC-NASA Resident Research Associate at NASA Langley Research Center. He is presently affiliated with Imperial College, London, England.

16. Abstract

The measurement of rotational temperature by the electron-beam fluorescence technique is investigated for temperatures between 78 K and 300 K by using the 0-0 band of the nitrogen first negative system. Existing methods for calculating the rotational temperature from electron-beam spectra result in values which are higher than the true temperature and the error increases with density and electron-beam current. The errors are believed to arise through neglect of the effects of secondary electrons. Excitation by low-energy secondary electrons can increase the population of the sparsely populated rotational ground states at the expense of the abundantly populated states. This secondary excitation is proposed as the cause of the error in the calculated rotational temperature and a theoretical study determines that the density and beam current govern the excitation rate. Rotational-temperature measurements are made in a flowing stream of nitrogen at a known temperature for a range of densities and beam currents. The product of density and beam current correlates the present data, and least-squares cubic polynomials are fitted through the temperature data as a function of this correlating parameter. An iterative procedure based on the polynomials allows more accurate rotational temperatures and, consequently, densities to be obtained with the electron-beam fluorescence technique. This procedure can be applied to measurements in some high-speed flow regimes.

17. Key Words (Suggested by Author(s))	18. Distribution Statement
Electron beam techniques Rotational temperature measurements Density measurements	Unclassified – Unlimited

19. Security Classif. (of this report)	20. Security Classif. (of this page)	21. No. of Pages	22. Price*
Unclassified	Unclassified	31	$3.00

*For sale by the National Technical Information Service, Springfield, Virginia 22151

ROTATIONAL-TEMPERATURE DETERMINATION IN FLOWING NITROGEN USING AN ELECTRON BEAM

By D. C. Lillicrap* and Louise P. Lee
Langley Research Center

SUMMARY

The measurement of rotational temperature by the electron-beam fluorescence technique is investigated for temperatures between 78 K and 300 K by using the 0-0 band of the nitrogen first negative system. Existing methods for calculating the rotational temperature from electron-beam spectra result in values which are higher than the true temperature and the error increases with density and electron-beam current. The errors are believed to arise through neglect of the effects of secondary electrons. Excitation by low-energy secondary electrons can increase the population of the sparsely populated rotational ground states at the expense of the abundantly populated states. This secondary excitation is proposed as the cause of the error in the calculated rotational temperature and a theoretical study determines that the density and beam current govern the excitation rate. Rotational-temperature measurements are made in a flowing stream of nitrogen at a known temperature for a range of densities and beam currents. The product of density and beam current correlates the present data, and least-squares cubic polynomials are fitted through the temperature data as a function of this correlating parameter. An iterative procedure based on the polynomials allows more accurate rotational temperatures and, consequently, densities to be obtained with the electron-beam fluorescence technique. This procedure can be applied to measurements in some high-speed flow regimes.

INTRODUCTION

As flight speeds are extended into the hypersonic regime, high recovery temperatures are encountered and can result in low-density regions within the flow field. The study of these regions with conventional probes may lead to unacceptably large errors. For instance, in high-speed low-density flows, corrections to pressure measurements for probe interference and orifice effects are large and difficult to apply, particularly in boundary layers close to the surface. Consequently, electron beams are used extensively

*NASA-NRC Research Associate, presently affiliated with Imperial College, London, England.

to study this flow regime since they have no appreciable effect on the flow, and measurements can be made to within a few mean free paths of the surface. (See ref. 1.) Interference-free measurements of this kind would be particularly valuable in the study of high Mach number turbulent boundary layers. In the low-density region close to the surface, it has been found (refs. 2 and 3) that the static pressure appears to increase significantly as the surface is approached. Wallace (ref. 4) used an electron-beam probe to determine mean and fluctuating densities in a turbulent boundary layer but the results were preliminary and temperature profiles were not measured. The potentially greater accuracy of interference-free electron-beam measurements of both density and temperature could provide a better understanding of the low-density regions of turbulent boundary layers.

The electron-beam fluorescence technique (ref. 5) consists of directing a collimated beam of moderate energy electrons through the flow field and, by use of a suitable optical system, of observing the fluorescence produced. This paper considers only density and rotational-temperature measurements in pure nitrogen. The intensity of the first negative bands can be related to the density and, if the rotational fine structure of a band is resolved, a rotational temperature can be obtained from the relative line intensities. For most conditions of interest, the rotational temperature equals the translational temperature and, in principle, the state of the gas can be determined at any point in the flow without appreciably disturbing the flow. (See ref. 1.) In practice, the rotational temperature calculated by using the equation derived by Muntz (ref. 5) is too high and the discrepancy increases with density and the number of spectral lines used (refs. 6 and 7). This discrepancy also leads to errors in determining the number density for conditions where quenching of the excited states through collisions is appreciable. (See ref. 8.)

The objective of this paper is to examine the possible causes of the high calculated rotational temperatures and hence remove some of the uncertainties associated with density and rotational-temperature measurements, particularly at the upper end of the density range where electron-beam techniques are applicable, on the order of 10^{23} molecules per meter^3. Excitation by low-energy secondary electrons is investigated, since it could result in a redistribution of the molecules among the ground-state rotational levels. An excitation model is proposed and the parameters affecting the calculated temperature are identified. The equations describing this excitation model involve unknown constants, and an experimental calibration of the technique for temperatures between 78 K and 300 K is performed for a range of densities and beam currents. An iterative procedure based on tabulated experimental results is developed to obtain more reliable values of rotational temperature and consequently density, provided certain conditions are satisfied.

SYMBOLS

A, B, C	constants
$B_{V_1''}$	rotational constant for V_1'' vibrational level
C_0, C_1, C_2, C_3	cubic polynomial coefficients
$\bar{C}$	mean molecular velocity
C_E	experimental constant
c	speed of light
F	excitation function
$F(K')$	defined by equation (19)
$f(v)$	secondary-electron velocity distribution function
G	defined by equation (2)
$g(v,\pm 2)_{K''}$	excitation cross section for secondary electrons
H	defined by equation (7)
h	Planck's constant
$I(K',K'')=I(K')=I\left(K',K_2''\right)$	intensity of K' rotational line
$I_{(0,0)}$	intensity of R branch of 0-0 band
i	beam current
J	defined by equation (8)
j	current density
K	rotational quantum number

K' rotational quantum number for $N_2^+B^2\Sigma$ state

K'' rotational quantum number for $N_2X^1\Sigma$ state

K_2'' rotational quantum number for $N_2^+X^2\Sigma$ state

K_{max} maximum number of spectral lines used

k Boltzmann constant

N nitrogen number density

$N_{K''}''$ number density of K'' level

$N_2^+B^2$ upper electronic state of nitrogen ion N_2^+

$N_2^+X^2$ ground state of nitrogen ion N_2^+

N_2X^1 ground state of nitrogen molecule N_2

n_s secondary electron number density

P_P relative rotational transition probability for P branch

P_R relative rotational transition probability for R branch

p beam diameter or field-of-view width

Q_R rotational state sum

$q\left(V', V_1''\right)$ Franck-Condon factor for transition between V' and V_1'' vibrational levels of two electronic states

$$R(T) = \left[\left(T_R\right)_{calc} / T_w\right]_T \Big/ \left[\left(T_R\right)_{calc} / T_w\right]_{300\ K}$$

$R_{K''}''$ net rate of secondary-electron excitation of K'' level

$r_{K''}$	rate of excitation of K' level by one transition
T	temperature
T_R	rotational temperature
T_w	wall temperature (equals static temperature)
V'	vibrational quantum number for $N_2^+B^2\Sigma$ state
V_1''	vibrational quantum number for $N_2X^1\Sigma$ state
v	electron velocity
v_o	reference electron velocity
$X(K')$	defined by equation (17)
$\Delta(K)$	change in rotational quantum number
$\Delta(K')$	change in upper state rotational quantum number
$\Delta(K'')$	change in ground-state rotational quantum number
$\Delta I(K')$	difference between experimental and theoretical rotational line intensities
δ	rarefaction parameter
θ	defined by equation (9)
λ_s	secondary-electron mean free path
ν	wave number of emitted radiation
Φ	rate of excitation defined by equation (5)

$\phi = B_{V_1''}hc/k$

Subscripts:

calc	calculated values defined by equation (11)
exp	experimental values
M	Maxwellian distribution
max	maximum value
min	minimum value
1,2	iteration approximations

THEORETICAL EXCITATION MODELS

Previous Models

To obtain the rotational temperature, Muntz (ref. 5) used a theoretical model to relate the measured rotational line intensities for the N_2^+ first negative bands to the undisturbed ground-state rotational distribution. He argued that primary electrons obeyed the optical dipole selection rules ($\Delta K = \pm 1$) in exciting the ground-state molecules directly to the $N_2^+B^2\Sigma$ state. This state decays spontaneously to the $N_2^+X^2\Sigma$ state and gives rise to the first negative system. If it is assumed that no other processes significantly affect the relative rotational line intensities, the excitation model leads to the equation

$$I(K',K'') = \text{Constant } \nu^4 K' G e^{-K'(K'+1)\phi/T_R} \tag{1}$$

where

$$G = \frac{(K' + 1)e^{-2(K'+1)\phi/T_R} + K'e^{2K'\phi/T_R}}{2K' + 1} \tag{2}$$

An iterative procedure is used to solve these equations for T_R, but the values obtained are too high. Robben and Talbot (ref. 9) first derived a correction curve for

$(T_R)_{calc}$ as a function of the temperature but subsequently, it was shown that the error in $(T_R)_{calc}$ also increased with density. (See refs. 6 and 7.) Secondary electrons, produced when the primary electrons ionized ground-state molecules, were suggested (refs. 10 and 11) as the cause of the high calculated temperatures. Some secondaries have sufficient energy to excite ground-state molecules to the $N_2^+B^2\Sigma$ state, but for these low electron energies, transitions for which $\Delta K = \pm 1, \pm 3, \pm 5, \ldots$ can occur. This condition results in high calculated temperatures, but order-of-magnitude calculations show that there are insufficient secondaries with the required energy to account for the large errors in $(T_R)_{calc}$. Furthermore, any appreciable direct excitation of the $N_2^+B^2\Sigma$ states by secondaries would result in a nonlinear variation of band intensity with density, even when quenching is negligible, as can be seen from reference 10. For low densities, less than 10^{22} molecules per meter^3, the band intensity varies linearly with density, and Maguire (ref. 7) used this variation to argue against secondary electron excitation in favor of preferential quenching of the rotational states. For this model to work, the quenching cross sections for the rotational states have to be a complicated function of the temperature and some states need to be strongly quenched even for densities less than 10^{22} molecules per meter^3. Yet another approach to this problem is the double excitation model proposed by Hickman (ref. 12) which allows transitions for $\Delta K = \pm 1$ and ± 3. Although the calculated temperatures are lower, this model offers no real advantage over Muntz's model.

Present Excitation Model

When a beam of moderate energy electrons passes through nitrogen, some of the ground-state molecules are ionized. The ions and secondary electrons diffuse out of the beam region, but the electrostatic field set up around the beam retards the electrons and results in high concentrations of secondary electrons. Beinkowski and Harbour (ref. 13), using a formalism similar to that of Self and Ewald (ref. 14) for a discharge column, calculated values several orders of magnitude larger than those derived previously with the electrostatic forces neglected. For a 10^{-3} meter beam radius and a 10^{-3}-ampere beam current in a gas at a density of 3.2×10^{22} molecules per meter^3, the estimated secondary-electron concentration was 4×10^{17} per meter^3. Harbour, Bienkowski, and Smith (ref. 15) subsequently measured concentrations close to the predicted values and an electron temperature of about 1 eV. For electrons of this energy, the cross section for excitation of ground-state rotational levels with a selection rule $\Delta K'' = \pm 2$ is

approximately 10^{-19} meter^2. (See ref. 16.) In view of the large secondary-electron concentrations and excitation cross sections, the effect on the ground-state rotational distribution function must be considered. The population of a particular ground state K'' is influenced by the net result of four transitions between it and the levels K'' = ±2, as illustrated in figure 1. These secondary transitions will cause a redistribution of the molecules among the ground-state rotational levels; thus, the population of the sparsely populated levels is increased at the expense of the more abundantly populated levels. This condition produces the effects observed by Maguire (ref. 7) without the need to assume that the abundantly populated $N_2^+B^2\Sigma$ states are preferentially quenched. The redistribution of the molecules will not appreciably change the total intensity of the first negative bands, and at low densities (less than 10^{22} molecules per meter^3), this model predicts a linear variation of intensity with density, as observed experimentally. Therefore, the objections to earlier modifications of Muntz's model (ref. 5) do not apply to this model, but further comparison with experiment requires a detailed study of the effect of the secondary electron excitation on the relative line intensities.

Figure 1 illustrates the complete excitation model by showing the transitions affecting the seventh rotational line. The K' = 7 level is populated by primary electrons from the K'' = 8 and K'' = 6 levels. Each of these levels is influenced by transitions excited by secondary electrons between them and adjacent even-numbered lines.

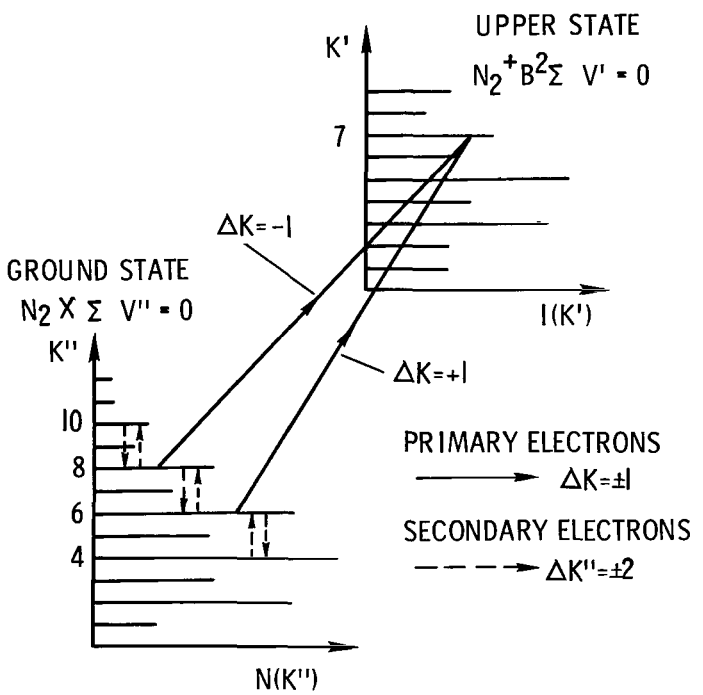

Figure 1.- Excitation model showing transitions for I(K' = 7).

To include the secondary-electron excitation, the perturbation of a particular K'' level is assumed to be proportional to the net rate of excitation of that level $R_{K''}$. Then,

$$N''_{K''} = \left(N''_{K''}\right)_M + CR''_{K''} \tag{3}$$

where C is a constant and the subscript M denotes the population for a Maxwellian distribution.

Order-of-magnitude calculations based on equation (3) predict an overpopulation of the higher rotational states compared with a Maxwellian distribution. Calculations are performed for unit volume occupied by a beam of diameter p, with the assumption that molecules enter and leave the beam only by thermal diffusion through the edge of the beam. The difference between the rate of diffusion out of the beam for a particular K'' level, and the rate of diffusion into the beam for the same level is the rate of excitation of that level per unit volume per second by the secondary electrons. It can be shown that

$$\frac{\bar{C}\left(N''_{K''}\right)_M}{p} + R''_{K''} = \frac{\bar{C}N''_{K''}}{p}$$

from which

$$\frac{pR''_{K''}}{\bar{C}\left(N''_{K''}\right)_M} + 1 = \frac{N''_{K''}}{\left(N''_{K''}\right)_M} \tag{4}$$

The expression for $R''_{K''}$ is developed later and depends on the density, secondary electron concentration, secondary electron energy, and corresponding excitation cross sections. Cross sections for 1 eV electrons were estimated to be two orders of magnitude greater than the values listed in reference 16 for 0.14 eV and are of the order of 10^{-19} meter^2. By using a secondary electron concentration n_s of 4×10^{17} per meter^3 from reference 13, equation (4) predicts a considerable overpopulation of the high rotational states. For example, at 78 K an overpopulation of approximately 30 percent is predicted for the eleventh rotational level. These order-of-magnitude calculations demonstrate that a more complete study of the proposed secondary-excitation mechanism is required.

To study the effect of secondary electrons in detail, the excitation by low-energy secondaries must be included in the equation for the relative rotational line intensities. Based on the Muntz method (ref. 5), the rate of excitation by primary electrons from

a V_1'' vibrational band to a K' level of the V' band of $N_2^+B^2\Sigma$ is

$$\Phi(V',K') = FNi \sum_{V_1''} \left\{ \left[\frac{N''_{K'+1}P_P + N''_{K'-1}P_R}{\sum_{K'} \left(N''_{K'+1}P_P + N''_{K'-1}P_R \right)} \right] q\left(V',V_1''\right) \right\} \tag{5}$$

per second per unit volume. In equation (5), F is the excitation function for an electron defined so that if all molecules are in the ground state, then FNi molecules are excited to the $N_2^+B^2\Sigma$ states per second per unit volume. (In the previously used notation (ref. 8), F was defined so that Fi molecules were excited to the $N_2^+B^2\Sigma$ states per second per unit volume. As a result, the so-called constants in the equations of ref. 8 involve the density.) For a Maxwellian distribution

$$\left(N''_{K''}\right)_M = N_{V_1''} \frac{2K'' + 1}{Q_R\left(T_R\right)_{V_1''}} e^{-K''(K''+1)\phi/T_R}$$

where $Q_R\left(T_R\right)_{V_1''}$ is the rotational state sum for the V_1'' level. Therefore, from equation (3)

$$N''_{K''} = N_{V_1''} \frac{2K + 1}{Q_R\left(T_R\right)_{V_1''}} e^{-K''(K''+1)\phi/T_R} + CR''_{K''}$$

Substituting for $N''_{K'+1}$ and $N''_{K'-1}$ in equation (5) and rearranging the equation yields

$$\Phi(V',K') = \frac{FNi}{\theta} \sum_{V_1''} \left\{ q\left(V',V_1''\right) \left[\frac{N_{V_1''}}{Q_R\left(T_R\right)_{V_1''}} H + J \right] \right\} \tag{6}$$

per second per unit volume. In equation (6)

$$\left.\begin{aligned} H &= (K' + 1)e^{-\left[(K'+1)(K'+2)\phi/T_R\right]} + K'e^{-\left[(K'-1)K'\phi/T_R\right]} \\ \phi &= 2.88 \end{aligned}\right\} \tag{7}$$

for the ground state of nitrogen and

$$J = C\left(R''_{K'+1}{}^{P}P + R''_{K'-1}{}^{P}R\right) \tag{8}$$

In reference 5, θ was introduced as a normalizing factor and is given by

$$\theta = \sum_{K'}\left(N''_{K'+1}{}^{P}P + N''_{K'-1}{}^{P}R\right) \tag{9}$$

The number densities in θ will not have a Maxwellian distribution among the ground states but this quantity is still a valid normalizing factor for a particular set of conditions.

At low temperatures there is no appreciable excitation of the vibrational levels of $N_2X^1\Sigma$ other than the $V''_1 = 0$ level so that $N_{\left(V''_1=0\right)} = N$. Therefore, for the 0-0 band, equation (6) becomes

$$\Phi(V' = 0,K') = \frac{FNiq(0,0)}{\theta}\left[\frac{NH}{Q_R\left(T_R\right)_{V''_1}} + J\right]$$

which for a given temperature and beam configuration, can be written as

$$\Phi(V' = 0,K') = \text{Constant } i\left[\frac{NH}{Q_R\left(T_R\right)_{V''_1}} + J\right]$$

where the constant is $\frac{FNq(0,0)}{\theta}$ per second per unit beam current and is independent of N since θ varies as N. By equating the rate of photon emission to the rate of excitation, Muntz (ref. 5) obtains the emission-time intensity from

$$I\left(K',K''_2\right)_{(0,0)} = \text{Constant } P\left(K',K'_2\right)\ \Phi(V' = 0,K')\ \nu^4$$

Substituting $P\left(K',K''_2\right) = P_R = K'/(2K' + 1)$ into this equation and treating ν^4 as a constant gives for the 0-0 band

$$I\left(K',K''_2\right)_{exp} = C_E i\left[\frac{N}{Q_R\left(T_R\right)_{V''_1}} K'Ge^{-K'(K'+1)\phi/T_R} + \frac{K'}{2K' + 1}J\right] \tag{10}$$

where G is given by equation (2) and C_E is a constant relating the experimental intensities to the theoretical intensities for a particular experiment. Define a function

$$I\left(K',K_2''\right)_{calc} = K'Ge^{-K'(K'+1)\phi/T_R} \tag{11}$$

Then equation (10) can be written as

$$I\left(K',K_2''\right)_{exp} = C_E i\left[\frac{N}{Q_R\left(T_R\right)_{V_1''}} I\left(K',K_2''\right)_{calc} + \frac{K'}{2K'+1} J\right] \tag{12}$$

The reader is referred to Muntz's paper (ref. 5) for more discussion of the steps leading to equation (12) since the present derivation is similar. The effect of secondary electrons on a particular K' level is introduced through J and depends on the rate of secondary excitation to the $K'' = K' \pm 1$ levels. The total intensity of the R or P branch of the band is not changed by the secondary excitation since one level is always populated at the expense of another level. Therefore, the sum over all K' of the terms involving J must be zero and from equation (12)

$$\sum_{K'}\left[I\left(K',K_2''\right)_{exp}\right] = C_E i \frac{N}{Q_R\left(T_R\right)_{V_1''}} \sum_{K'}\left[I\left(K',K_2''\right)_{calc}\right]$$

Let

$$\left[I_{(0,0)}\right]_{exp} = \sum_{K'} I\left(K',K_2''\right)_{exp}$$

and

$$\left[I_{(0,0)}\right]_{calc} = \sum_{K'} I\left(K',K_2''\right)_{calc}$$

Then

$$\left[I_{(0,0)}\right]_{exp} = C_E i \frac{N}{Q_R\left(T_R\right)_{V_1''}}\left[I_{(0,0)}\right]_{calc}$$

Normalizing equation (12) by $\left[I_{(0,0)}\right]_{exp}$ yields

$$\left[\frac{I(K')}{I_{(0,0)}}\right]_{exp} = \left[\frac{I(K')}{I_{(0,0)}}\right]_{calc} + \frac{K'JQ_R\left(T_R\right)_{V_1''}}{(2K' + 1)N\left[I_{(0,0)}\right]_{calc}} \tag{13}$$

where only the upper state quantum number K' denotes the rotational line.

To evaluate J, values of $R''_{K''}$ are required for each ground-state rotational level. The selection rule for transitions produced by the low-energy electrons is $\Delta K'' = \pm 2$ and $R''_{K''}$ is the net value for the transitions between levels K'' and $K'' \pm 2$. The cross sections are denoted by $g(v,\pm 2)_{K''}$ where the subscript denotes the level from which the transition arises and (± 2) is $\Delta K''$.

When the excitation of the K'' level from the $K'' - 2$ level is considered, the rate of excitation by secondary electrons is

$$r_{K''} = n_s N''_{K''-2} \int_v g(v,+2)_{K''-2} f(v)\, v\, dv$$

per unit volume per second. To avoid the integral over the unknown $f(v)$, the cross section $g(v,+2)_{K''-2}$ is written in terms of the value for a reference velocity v_o and all the cross sections are assumed to vary in a similar manner with velocity. This variation does not seem to be unreasonable from the values given in reference 16. Then

$$r_{K''} = n_s N''_{K''-2} g\left(v_o,+2\right)_{K''-2} \int_v \frac{g(v,+2)_{K''-2}}{g\left(v_o,+2\right)_{K''-2}} f(v)\, v\, dv$$

Within the accuracy of this assumption, the integral is the same for all K'', can be treated as a constant, and allows the calculation of relative values for $r_{K''}$. Thus,

$$r_{K''} = \text{Constant } n_s N''_{K''-2} g\left(v_o,+2\right)_{K''-2} \tag{14}$$

per unit volume per second.

The rate of excitation required is that due to transitions within the observed gas volume. For a field of view of the optics larger than the beam diameter, the beam size determines this volume. For large or scattered beams, the field of view of the optics usually determines this volume. If p is the beam diameter or field-of-view width, the dependence of $r_{K''}$ on number density is different for the two limits $\lambda_s > p$ and $\lambda_s < p$. For $\lambda_s < p$, the excitation rate is given by equation (14) but for $\lambda_s > p$, the

probability of a secondary electron colliding within the observed volume increases as N and $r_{K''} \approx Nn_s N''_{K''-2} g(v_o,+2)_{K''-2}$. The excitation rate $R_{K''}$ is the net result of $r_{K''}$ for four transitions and for $\lambda_s > p$ and is

$$R_{K''} = \text{Constant } Nn_s \left\{ N''_{K''+2} g(v_o,-2)_{K''+2} + N''_{K''-2} g(v_o,+2)_{K''-2} - N''_{K''} \left[g(v_o,+2)_{K''} + g(v_o,-2)_{K''} \right] \right\}$$

Substituting values of $R_{K''}$ into equation (13) and writing the result in terms of K' gives for $\lambda_s > p$

$$\left[\frac{I(K')}{I_{(0,0)}}\right]_{exp} = \left[\frac{I(K')}{I_{(0,0)}}\right]_{calc} + \frac{An_s K' Q_R (T_R)_{V''_1}}{\left[I_{(0,0)}\right]_{calc} (2K'+1)} \left\{ \frac{(K'+1)\left[X(K'+1)\right]}{2K'+3} + \frac{K'\left[X(K'-1)\right]}{2K'-1} \right\} \tag{15}$$

and, similarly, for $\lambda_s < p$

$$\left[\frac{I(K')}{I_{(0,0)}}\right]_{exp} = \left[\frac{I(K')}{I_{(0,0)}}\right]_{calc} + \frac{Bn_s K' Q_R (T_R)_{V''_1}}{N\left[I_{(0,0)}\right]_{calc} (2K'+1)} \left\{ \frac{(K'+1)\left[X(K'+1)\right]}{2K'+3} + \frac{K'\left[X(K'-1)\right]}{2K'-1} \right\} \tag{16}$$

where A and B are constants and

$$X(K') = N''_{K'-2} g(v_o,+2)_{K'-2} + N''_{K'+2} g(v_o,-2)_{K'+2} - N''_{K'} \left[g(v_o,+2)_{K'} + g(v_o,-2)_{K'} \right] \tag{17}$$

A first approximation to $X(K')$ can be obtained by substituting Maxwellian values for $N''_{K''}$; this substitution gives

$$X(K') = \frac{N}{Q_R(T_R)_{V_1''}} F(K') \tag{18}$$

where

$$F(K') = g\left(v_o,+2\right)_{K'-2}\left[(2K' - 3)e^{-(K'-2)(K'-1)\phi/T_R}\right]$$

$$+ g\left(v_o,-2\right)_{K'+2}\left[(2K' + 5)e^{-(K'+2)(K'+3)\phi/T_R}\right]$$

$$- (2K' + 1)e^{-K'(K'+1)\phi/T_R}\left[g\left(v_o,+2\right)_{K'} + g\left(v_o,-2\right)_{K'}\right] \tag{19}$$

Substituting for $X(K')$ in equations (15) and (16) gives for $\lambda_s > p$

$$\left[\frac{I(K')}{I_{(0,0)}}\right]_{exp} \approx \left[\frac{I(K')}{I_{(0,0)}}\right]_{calc}$$

$$+ \frac{An_sNK'}{\left[I_{(0,0)}\right]_{calc}(2K' + 1)}\left[\frac{K' + 1}{2K' + 3} F(K' + 1) + \frac{K'F(K' - 1)}{2K' - 1}\right] \tag{20}$$

and for $\lambda_s < p$

$$\left[\frac{I(K')}{I_{(0,0)}}\right]_{exp} \approx \left[\frac{I(K')}{I_{(0,0)}}\right]_{calc}$$

$$+ \frac{Bn_sK'}{\left[I_{(0,0)}\right]_{calc}(2K' + 1)}\left[\frac{(K' + 1)F(K' + 1)}{2K' + 3} + \frac{K'F(K' - 1)}{2K' - 1}\right] \tag{21}$$

For the proposed excitation model, equations (20) and (21) predict that the difference between the measured line intensities and values calculated from Muntz's equation (ref. 5) varies as Nn_s at low densities $\left(\lambda_s > p\right)$ and tends to a dependence on n_s at high densities $\left(\lambda_s < p\right)$. The transition from one regime to the other occurs for $\lambda_s \approx p$

and therefore at a density which depends on the geometry of the electron beam and optical system. At the present time n_s cannot be reliably evaluated as a function of the gas density. Estimates can be made of the increase in n_s due to the electrostatic field set up around the beam (ref. 13), but the quantitative effects of beam spreading and the recombination of electrons with ions are unknown. In addition, the constants A and B involve the integral over the secondary electron distribution function and cannot be reliably evaluated.

The value of equations (20) and (21) is the predicted dependence of the normalized line intensities, and hence the calculated rotational temperature, on the gas density, secondary electron number density, and beam geometry. Experimental measurements are needed to confirm these predictions and to provide a calibration of the technique for a range of temperatures and densities.

MEASURED ROTATIONAL TEMPERATURES

The experimental measurements were made in a flowing stream of nitrogen at a known temperature using a 30 keV electron beam and beam currents between 0.3 and 1.5 mA. The impurity level in the nitrogen was 50 parts per million. Figure 2 shows the heat exchanger used to cool the gas and the position of the electron beam.

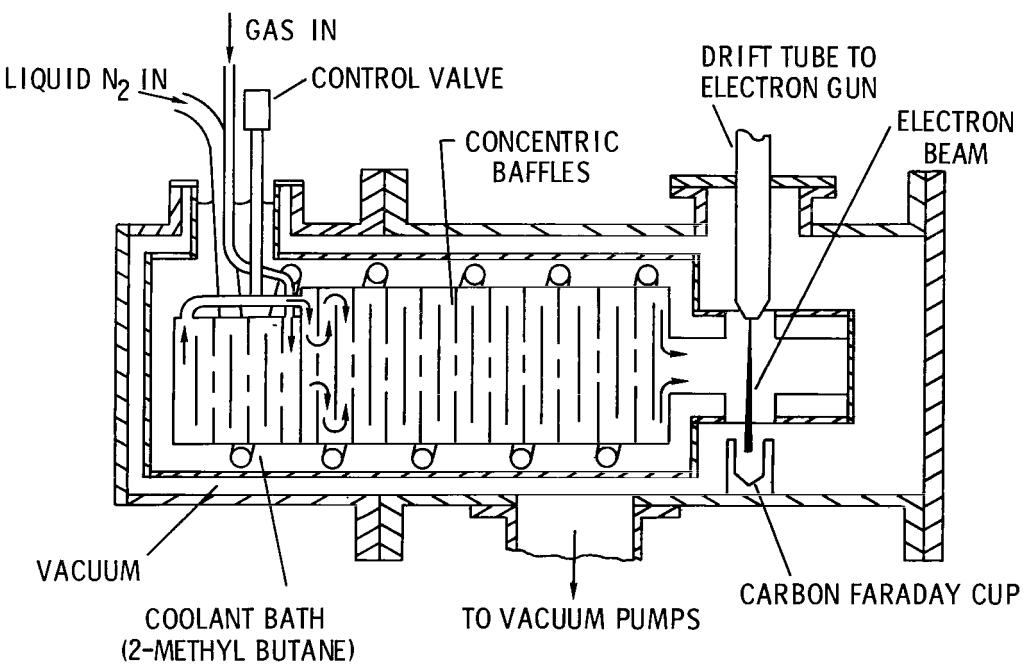

Figure 2.- Schematic diagram of test chamber.

The heat exchanger is enclosed in a bath of 2-methyl butane which is thermally insulated by the surrounding vacuum. A controlled flow of liquid nitrogen through a coil immersed in the 2-methyl butane permits the cooling of the heat exchanger to any desired temperature between 300 K and 113 K. Alternatively, liquid nitrogen is used in place of a 2-methyl butane to obtain temperatures close to 78 K. The heat exchanger consists of two chambers separated by a valve which controls the pressure in the first chamber. This chamber acts as a reservoir of cooled gas for the main chamber to insure that the gas is cooled to the temperature of the heat exchanger, even at the lowest pressures. The gas temperature is assumed to be the mean value recorded by thermocouples on the last baffle and along the exit pipe from the heat exchanger. The diameter of the exit pipe was 32 mm and the pumps maintained a maximum velocity through it of approximately 50 m/sec which is sufficient to prevent convective heating of the gas by the hot drift tube and mixing with the warmer gas from the surrounding chamber. (See ref. 8.)

A calibrated pressure transducer recorded the test chamber pressure through an orifice in the chamber wall. The wall temperature remains close to ambient and thermal transpiration along the tubing is negligible. The density of the flowing gas is calculated from the measured pressure and temperature.

The electron beam enters the test region through a narrow orifice in the drift tube. For pressures below 130 N/m^2, the orifice diameter is 0.1 cm but for higher pressures is 0.05 cm. Both drift tube and electron gun are insulated from ground potential and a grounded shield leaves only a small circular area around the drift tube orifice exposed. To measure beam current, the whole test chamber served as the collector and the carbon Faraday cup reduced the backscatter of primary electrons from the chamber walls. This procedure avoids errors due to beam spreading that arise when only the Faraday cup is used as the beam collector.

Measurements showed that at high beam currents the nitrogen first negative band intensities did not vary linearly with beam current, particularly for the higher densities and smaller drift tube orifice. The nonlinearity is thought to be due to an interaction between the drift tube and the plasma produced by the beam in and around the end of the drift tube orifice. The drift tube is slightly positive with respect to ground potential and draws a net electron current from the plasma. Unbalanced positive ions left in the plasma diffuse to the test chamber walls and thus reduce the indicated electron-beam current below the true value. This problem is discussed in reference 8 and leads to errors for high beam currents at high densities, but these errors do not seriously affect the conclusions of this study.

An optical system formed a 1:1 image of the beam on the entrance slit of a spectrometer which resolved all the lines in the R branch of the 0-0 band. The slit length, oriented perpendicular to the length of the beam image, determined the width of the field

of view of the optics. This width was 0.1 cm on either side of the beam center line, unless otherwise stated. The slit width determined the resolution along the length of the beam so that the volume of gas observed depends on the slit area and the depth of focus of the optical system. At low densities, when beam spreading is small, the fluorescence is observed from a cylindrical volume defined by the intersection of the field of view with the beam. For higher densities some of the electrons are scattered beyond the field of view (ref. 8). Fluorescence is then observed from a section through the beam of almost constant width determined by the slit length. Measurements were made at selected temperatures for a range of densities by scanning the rotational lines while measuring the total fluorescence intensity to monitor for changes in pressure or beam current.

Figure 3 shows the influence of beam current and density on the measured rotational temperature at 125 K. The symbols denote the values for a fixed density with variable beam current, and Ni correlates the ratio $(T_R)_{calc}/T_w$ for the limited range of beam currents. The solid line is a cubic polynomial fitted through the points by the least-squares method. It is noted that $(T_R)_{calc}/T_w$ does not approach 1.0 as Ni tends to zero and it increases to an almost constant value for $Ni > 6 \times 10^{25}$ microamperes × molecules per meter^3.

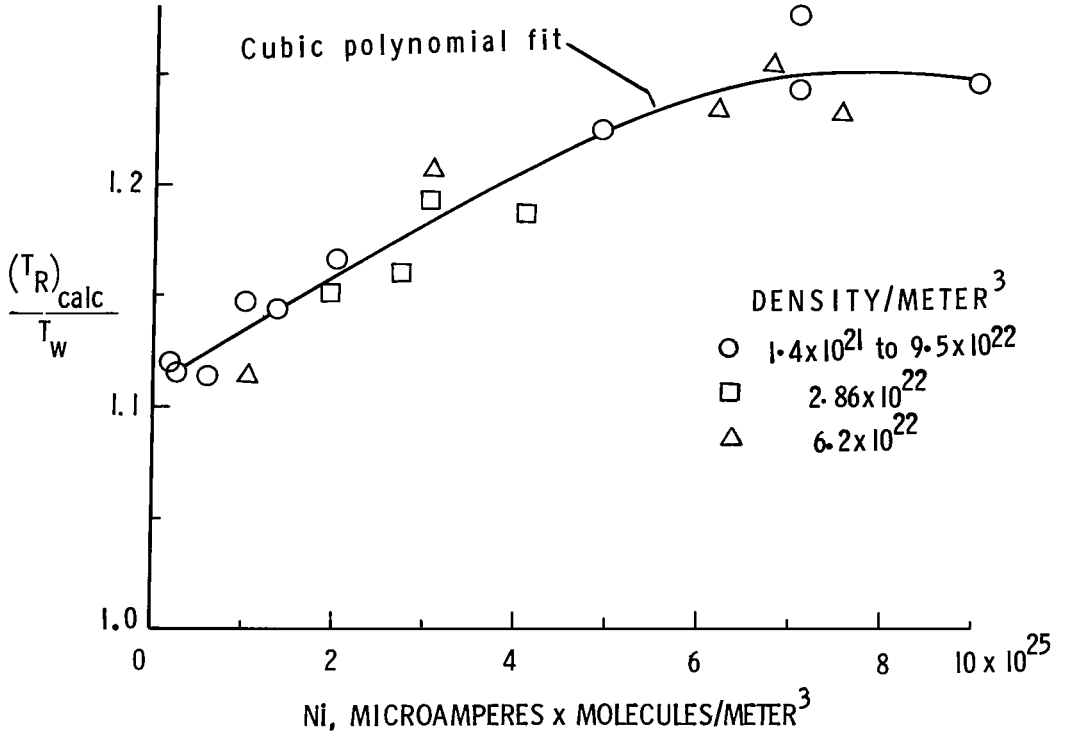

Figure 3.- Calculated rotational temperature against Ni. $K_{max} = 15$, $T_w = 125$ K.

The present results for other temperatures are similar to those presented in figure 3. The ratio $(T_R)_{calc}/T_w$ increases with density and reaches an almost constant level at high densities. This level decreases with increasing temperature.

DISCUSSION

Equations (20) and (21) predict that $\Delta I(K')/\left[\bar{I}_{(0,0)}\right]_{calc}$ varies as $n_s N$ at low densities $(\lambda_s > p)$ and tends to a dependence on n_s at high densities $(\lambda_s < p)$. Figure 4 shows $\left[\bar{I}(K')/I_{(0,0)}\right]_{exp}$ for two rotational levels at 111 K plotted against Ni. At high densities $\left[\bar{I}(K')/I_{(0,0)}\right]_{exp}$, and hence $\Delta I(K')/\left[\bar{I}_{(0,0)}\right]_{calc}$, varies linearly with Ni and at low densities it varies approximately N times faster, as predicted by equations (20) and (21). The transition between the two regimes occurs for a number density of approximately 1.5×10^{22} per meter^3, corresponding to a total collision cross section of 3×10^{-19} meter^2 which is the same order of magnitude as that given by Takayanagi et al. (ref. 16) for electrons of 1 eV energy. Furthermore, I(3) originating from the abundantly populated rotational levels is reduced and I(13) originating from the

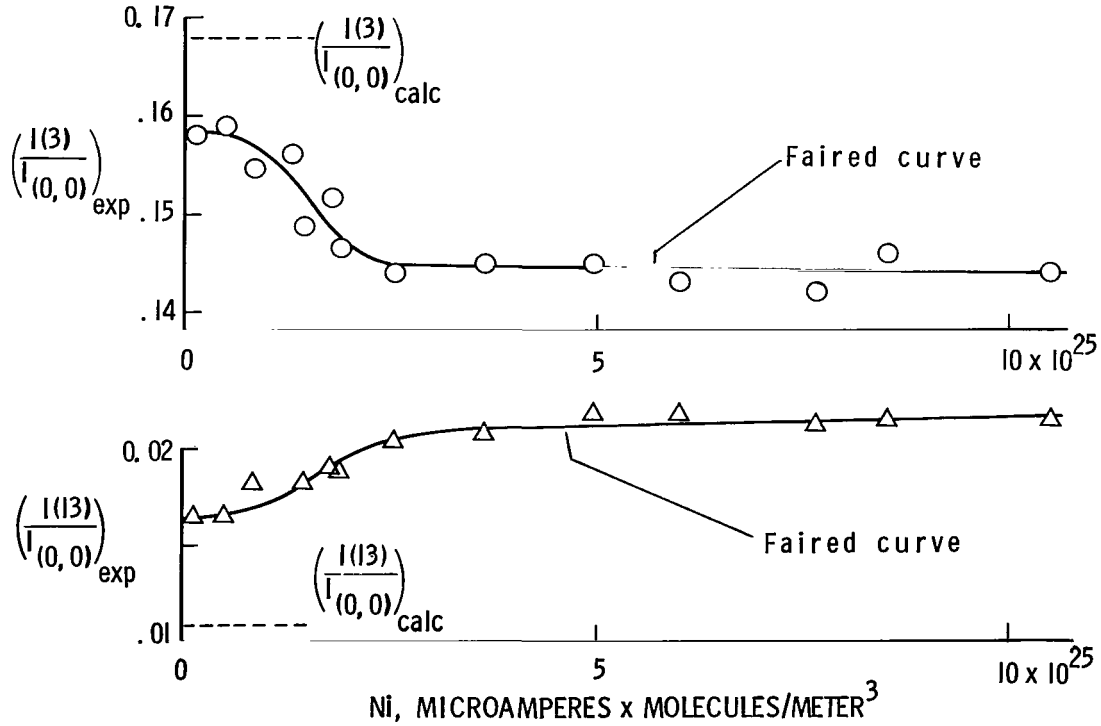

Figure 4.- Normalized line intensities. T = 111 K.

sparsely populated levels is increased. Similar trends observed for all the present data strongly support the assumption of low-energy secondary electron excitation of the ground-state rotational levels.

The ratio $\left[I(K')/I_{(0,0)}\right]_{exp}$ does not tend to $\left[I(K')/I_{(0,0)}\right]_{calc}$ as N tends to zero for the present measurements. This condition could be due to some unaccounted for secondary effect or to the variation of n_s with density. Dunn and Self (ref. 17) state that for $N < 3 \times 10^{18}$ molecules per meter^3, the beam-generated plasma is typically of about the same density as the beam. At higher densities, the electrostatic forces become important and references (13) and (15) show that n_s is increased by several orders of magnitude for $N = 3 \times 10^{19}$ molecules per meter^3. Therefore, n_s must increase rapidly with density for $3 \times 10^{18} < N < 3 \times 10^{19}$ molecules per meter^3. All the present results are for higher densities and would therefore appear to tend to the wrong limit when plotted against Ni.

The potential distribution in the beam-generated plasma governs the distribution of n_s (refs. 13 and 17) but the magnitude of n_s depends on the rate of production of secondary electrons and ions by the primary beam. Although the total beam current does not change greatly, the distribution of current density j changes with beam length and density because of the spreading of the beam through collisions. Therefore, unless the distribution of n_s is independent of the distribution of j, the present measurements at a distance of 2.8 cm along the beam should reflect the variation of j with density. The ratio $I(K')/I_{(0,0)}$ varies approximately as N^2i, tends to Ni at high densities, and thus implies that over the observed area of the beam, n_s does not depend on the distribution of j but only on the total rate of production of secondary electrons which is proportional to Ni. The solution of Bienkowski and Harbour (ref. 13) implies that this concept should be approximately true since the secondary electron number density at the beam center tends to become independent of beam diameter for large ratios of chamber to beam diameter.

This point is of major importance in any attempt to correct rotational temperature measurements by using curves of $(T_R)_{calc}/T_w$ against Ni. If n_s is not independent of the distribution of j, then the ratio $(T_R)_{calc}/T_w$ would vary along the length of the beam. The reasonable agreement of the present results (figs. 5 and 6) with those of other investigators (refs. 6 and 18) and the evidence of figure 4 suggest that n_s is approximately independent of the distribution of j at least for moderate beam lengths.

Figure 4 shows that there are three density regimes to consider. For $N < 3 \times 10^{19}$ molecules per meter^3, a rapid increase in n_s with density is thought to

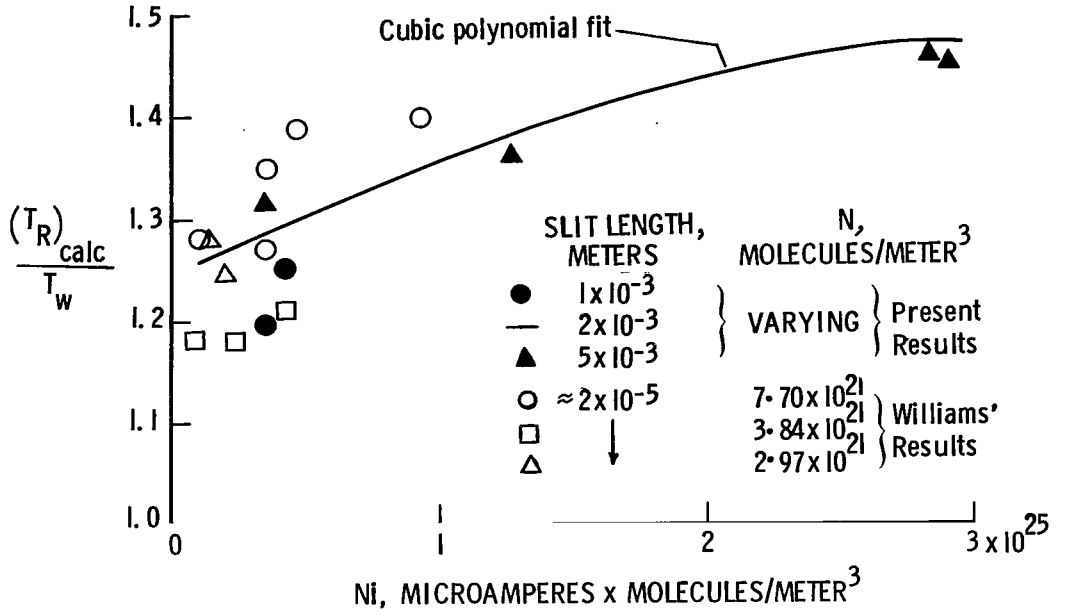

Figure 5.- Comparison with Williams' result at 78 K. K_{max} = 15.

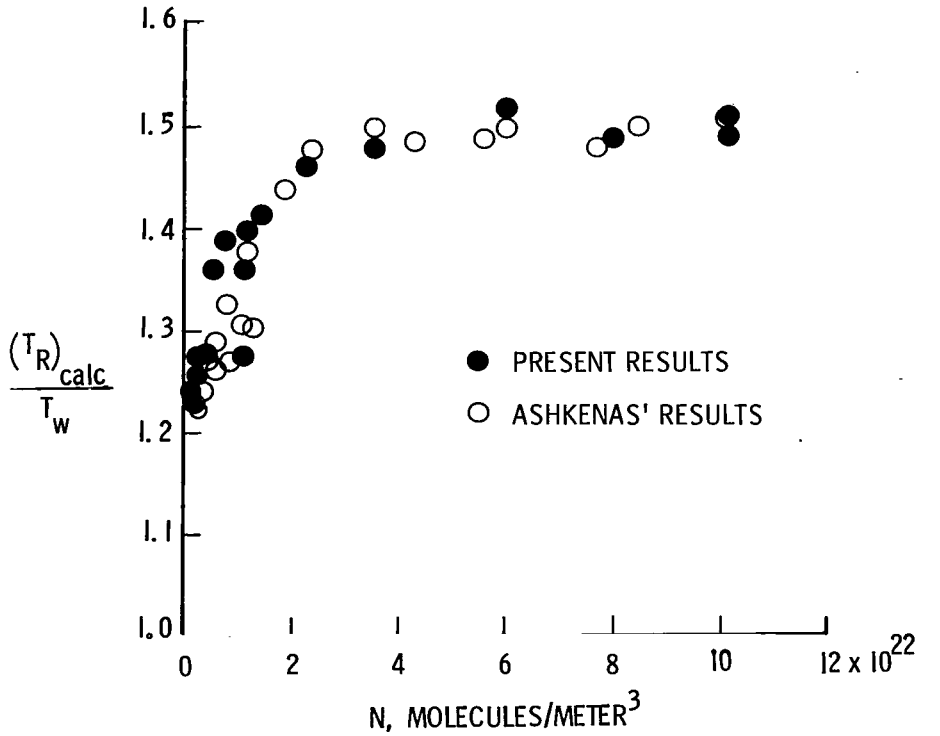

Figure 6.- Comparison with Ashkenas' results at 78 K using 15 rotational lines.

be responsible for the large values of $\Delta I(K')/\left[I_{(0,0)}\right]_{calc}$, and hence high $(T_R)_{calc}/T_w$, even at the lowest densities reached in the present experiment. For higher densities, n_s increases approximately linearly with Ni and the mean free path of the electrons varies as 1/N. Therefore, when $\lambda_s > p$, the number of secondary electrons colliding within the observed volume increases as N, and results in $\Delta I(K')/\left[I_{(0,0)}\right]_{calc}$ increasing approximately as N^2i. For $\lambda_s < p$, all the electrons are observed and $\Delta I(K')/I_{(0,0)}$ increases as Ni. This result explains the variation of $(T_R)_{calc}/T_w$ which should be a function of Ni when $\lambda_s < p$ and a function of N^2i when $\lambda_s > p$. The correlation of the data in figure 3 with Ni for the complete density range is not understood, but the range of beam currents is not large.

When $\lambda_s < p$, the geometry of the electron beam and optical system are less important since practically all the secondary electrons produced within the observed volume collide within that volume and $(T_R)_{calc}/T_w$ increases only very slowly with Ni. However, when $\lambda_s \geqq p$, the geometry determines how many secondary electrons collide within the observed volume and hence the rate at which $(T_R)_{calc}/T_w$ approaches the almost constant value for $\lambda_s < p$; therefore, for low densities, increasing the slit length should increase $(T_R)_{calc}/T_w$. Figure 5 compares $(T_R)_{calc}/T_w$ measured at 78 K for different spectrometer slit lengths. The limited amount of data and the experimental scatter precludes any definite conclusion, but $(T_R)_{calc}/T_w$ appears to increase slightly with slit length. Petrie et al. (ref. 19) observed a similar effect of slit length in a Mach 11 flow with static temperatures for 20 K and 35 K. Williams (ref. 18) also made measurements at 78 K but in his case the slit dimension, in the direction perpendicular to the beam length, appears to be 2×10^{-5} meter. The experimental scatter is too large to draw any conclusion about the effect of the small slit dimension but the results are scattered about the present data and increase with Ni.

Ashkenas (ref. 6) measured rotational temperatures at 78 K and room temperature but did not state what beam currents were used. The maximum beam current for his data (ref. 6) appears to be 3.5×10^{-4} ampere, whereas for the present results it was a maximum of 1.5×10^{-3} ampere and decreases to about one-fifth of this value at high densities. When $\lambda_s < p$, $(T_R)_{calc}/T_w$ is insensitive to Ni and therefore these differences in beam current should not be important. This result is confirmed in figure 6 which compares the results for 78 K plotted against density only. At low densities $(\lambda_s > p)$, the experimental scatter prevents different trends in the two sets of data from being detected.

In principle, equation (15) or (16) allows the relative values of $\Delta I(K') \Big/ \left[\overline{I}_{(0,0)}\right]_{calc}$ to be evaluated, but the secondary-electron excitation redistributes the molecules among the ground-state rotational levels and $N''_{K''}$ is not known. A first approximation can be obtained by assuming a Maxwellian distribution which leads to equations (20) and (21). With equation (19), either equation (20) or (21) gives values of $\Delta I(K')/-\Delta I(3)$ as a function of K' only, and these values are compared with experimental values in figures 7 and 8. Quantitative agreement is not expected because of non-Maxwellian distribution, but the qualitative agreement is very good and sparsely populated levels are populated at the expense of the more abundantly populated levels. Qualitative agreement at higher temperatures is equally good and, as the peak in the rotational distribution moves toward higher K'', the depopulation of successively higher rotational states is predicted and agrees with the data. At temperatures of several hundred K, the low rotational states have relatively low populations and secondary electron excitation would increase their population at the expense of the higher states. This increase leads to low values of $(T_R)_{calc}$ and could explain Hunter's (ref. 20) results at high temperatures, but the report does not state which rotational lines were used.

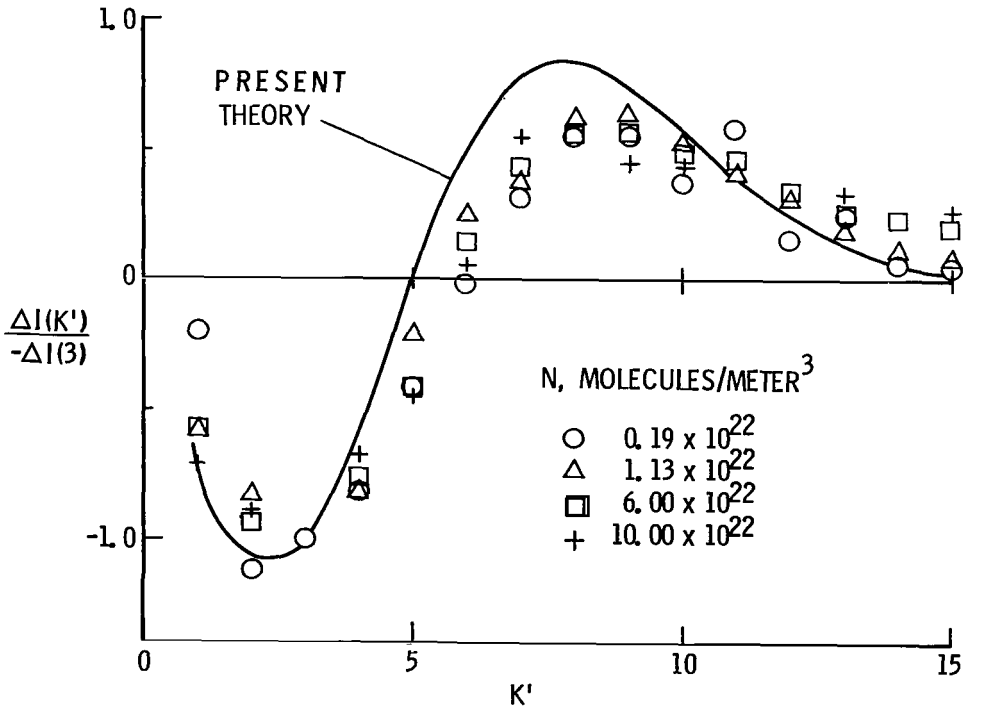

Figure 7.- Relative intensity error at 79 K.

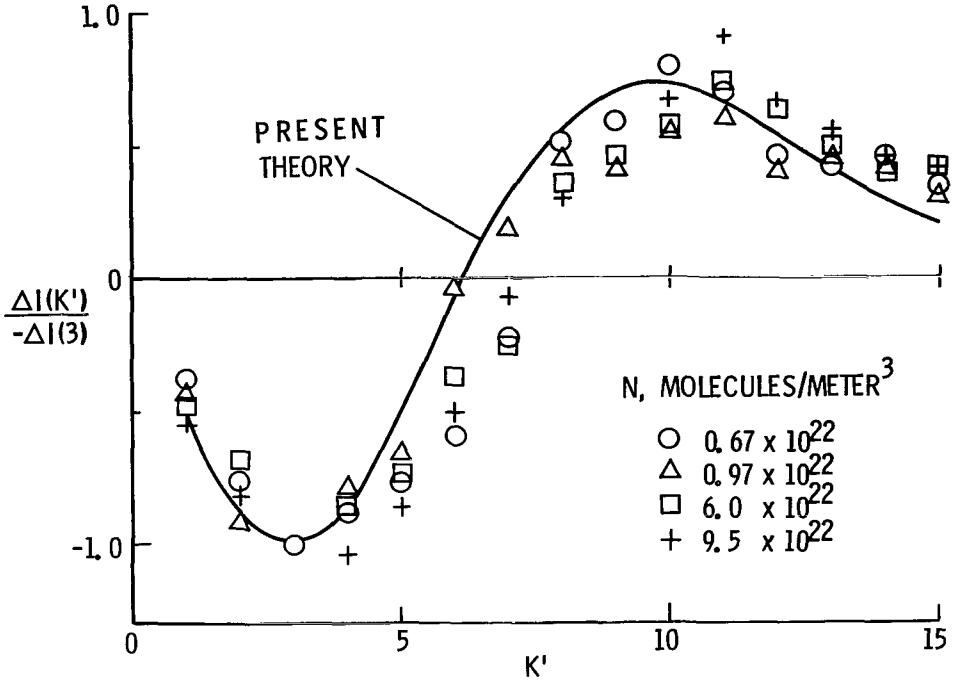

Figure 8.- Relative intensity error at 125 K.

Aerodynamic Measurements

An important use of the electron-beam fluorescence probe is the study of high Mach number low-density aerodynamics and consideration must be given to the effect of high flow velocities. The present results strongly support the hypothesis of excitation of ground-state rotational levels by low-energy secondary electrons. The qualitative effect of high flow velocities on this model can be deduced by reference to the rarefaction parameter δ defined by Bienkowski and Harbour (ref. 13) as the ratio of the beam radius to a modified mean free path. High velocities can only affect the $(T_R)_{calc}/T_w$ through the distribution of n_s since the rate of production by primary electrons is independent of velocity. Collisions between fast-moving neutral molecules and ions in the beam will sweep the ions downstream and the electrostatic attraction between ions and electrons causes a redistribution of the secondary electrons. Bienkowski and Harbour (ref. 13) concluded that for $\delta \leqq 1$, there should be little effect of velocity, but for $\delta >> 1$, the distribution of n_s, and hence $(T_R)_{calc}/T_w$, is affected. A value of δ of 1 corresponds to approximately 10 N/m^2 at room temperature for many electron-beam situations and most of the present results are in the regime where $\delta \geqq 1$.

Comparison of the present results with wind-tunnel measurements for known flow conditions and similar beam parameters would determine the effect of flow velocity.

Measurements are available in a Mach 6 flow (ref. 21) for a static temperature of 71.5 K and δ of order 1. Extrapolating the present results to this temperature gives $\left(T_R\right)_{calc}/T_w = 1.13 \pm 0.03$ compared with 1.09 ± 0.03 for the wind-tunnel data; thus, it is confirmed that there is little effect of the velocity for $\delta \approx 1$. For all other known wind-tunnel measurements, there are either geometric differences or the beam currents are not given. In addition, there is some doubt about Ni as a correlating parameter. If a beam current of 4.5×10^{-3} ampere is assumed, the Mach 9 data of Williams, Hornkohl, and Lewis (ref. 22) agree with the present data to within 6 percent. Their Mach 10 data are considerably higher, possibly because of uncertainties in the flow conditions. The Mach 3.92 data of Robben and Talbot (ref. 9) for a beam current of 10^{-2} ampere are very much lower than the present results for the same Ni but show reasonable agreement when compared only in terms of the density. Maguire's free-jet measurements at 154 K (ref. 7) cover a range of densities for $\delta > 1$, but the beam currents were not given and the slit was parallel to the beam image. The effect of the different geometric arrangement is less important at high densities, and for $N = 1.23 \times 10^{23}$ molecules per meter^3, Maguire's result is 4 percent lower than that of the present study. This difference shows that there is no strong effect of flow velocity on $\left(T_R\right)_{calc}$. Such a result is to be expected since $\left(T_R\right)_{calc}/T_w$ is insensitive to n_s at high densities $\left(\lambda_s << p\right)$ and therefore to the influence of flow velocity on the distribution of n_s. For lower densities, the discrepancies increase to 10 percent for $N = 1.32 \times 10^{22}$ molecules per meter^3, but no conclusion can be drawn because of the different geometries.

Correction Procedure for $\left(T_R\right)_{calc}$

Many variables influence $\left(T_R\right)_{calc}$ and simple correction procedures will apply only for specific conditions. The present measurements used beam currents of approximately 10^{-3} ampere and a field of view of the optical system of 0.1 cm on either side of the beam center line. The drift tube orifice was 0.1 cm or 0.05-cm diameter, but the beam spreads beyond this at the measurement station which is 2.8 cm from the drift tube. A correction procedure using curves of $\left(T_R\right)_{calc}/T_w$ as a function of Ni will apply only for beam currents for which the correlating parameter Ni is valid. The results might be different for beam lengths considerably greater than 2.8 cm, and at low densities $\left(\lambda_s > p\right)$, the field of view is important.

For each set of data at a fixed temperature T_w, a least-squares cubic polynomial was fitted through the values of $\left(T_R\right)_{calc}/T_w$ as a function of Ni. The polynomial

TABLE I.- POLYNOMIAL COEFFICIENTS FOR $(T_R)_{calc}/T_w$

	Coefficients for T of –							
	79 K	111 K	125 K	167 K	210 K	237 K	258 K	300 K
$K_{max} = 15$								
C_0	1.226	1.103	1.110	1.047	1.028	1.054	1.002	1.014
$C_1 \times 10^{27}$	15.11	9.86	2.24	2.66	4.20	2.42	8.85	11.69
$C_2 \times 10^{53}$	-22.69	-16.0	1.30	0.174	-4.71	-1.83	-25.81	-37.52
$C_3 \times 10^{79}$	11.65	8.85	-2.37	-2.07	1.95	0.246	25.12	36.2
$K_{max} = 14$								
C_0	1.193	1.091	1.106	1.037	1.025	1.054	1.007	1.015
$C_1 \times 10^{27}$	13.36	8.84	0.597	3.40	4.46	2.26	7.7	11.15
$C_2 \times 10^{53}$	-22.71	-15.3	4.82	-2.15	-5.36	-0.850	-20.61	-37.52
$C_3 \times 10^{79}$	12.74	9.23	-4.64	-0.224	2.30	-0.920	18.58	33.72
$K_{max} = 13$								
C_0	1.162	1.105	1.093	1.035	1.025	1.063	1.023	1.016
$C_1 \times 10^{27}$	12.81	6.14	1.45	3.51	4.64	1.77	5.23	10.68
$C_2 \times 10^{53}$	-24.06	-9.46	2.35	-1.44	-5.73	-0.373	-11.20	-34.55
$C_3 \times 10^{79}$	14.45	5.41	-2.89	-1.19	2.51	-0.623	8.78	34.18
$K_{max} = 12$								
C_0	1.142	1.126	1.103	1.020	0.992	1.054	1.033	1.022
$C_1 \times 10^{27}$	11.81	4.00	0.345	3.78	7.82	1.66	5.13	10.22
$C_2 \times 10^{53}$	-23.07	-6.03	0.438	-2.46	-13.23	0.898	-14.05	-34.28
$C_3 \times 10^{79}$	14.06	3.88	-4.09	-0.217	7.58	-2.27	13.55	34.77
$K_{max} = 11$								
C_0	1.121	1.126	1.075	0.995	0.978	1.042	0.996	1.007
$C_1 \times 10^{27}$	11.77	2.83	2.54	5.11	7.67	2.22	8.81	11.04
$C_2 \times 10^{53}$	-24.34	-2.07	-0.581	-4.82	-12.7	2.65	-24.97	-34.06
$C_3 \times 10^{79}$	15.37	0.401	-0.954	1.26	7.55	-5.69	23.40	32.22
Range of Ni, $\frac{\text{microamperes} \times \text{molecules}}{\text{meter}^3}$								
$(Ni)_{max}$	1×10^{26}	7.7×10^{25}	9×10^{25}	7.2×10^{25}	8×10^{25}	7.2×10^{25}	6×10^{25}	6×10^{25}
$(Ni)_{min}$	7.8×10^{23}	1.5×10^{24}	2×10^{24}	2×10^{24}	2×10^{24}	1×10^{24}	1.3×10^{24}	6.4×10^{22}

coefficients are given in table I, where K_{max} is the number of spectral lines used except for 300 K, when the first two lines were neglected because of overlapping by the P branch. Within the range of Ni given at the bottom of this table for each temperature, values of $(T_R)_{calc}/T_w$ can be calculated from

$$(T_R)_{calc}/T_w = C_0 + C_1 Ni + C_2(Ni)^2 + C_3(Ni)^3$$

Values of $(T_R)_{calc}/T_w$ calculated from these polynomials are plotted in figure 9 for selected values of Ni.

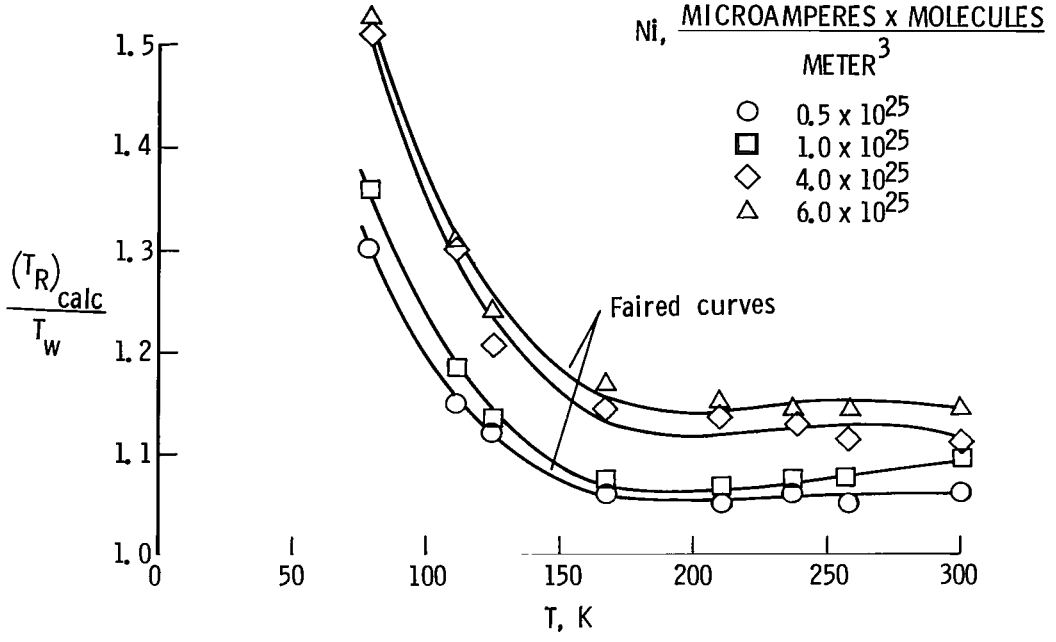

Figure 9.- Mean values of $(T_R)_{calc}/T_w$ computed from polynomials. $K_{max} = 15$.

The calculated rotational temperature depends on the density, but to measure density when quenching is appreciable, the temperature must be known and an iterative procedure is required to correct the measurements. (See ref. 8.) First estimates are made of T_1 and N_1 and equation (1) used to calculate $(T_R)_{calc}$ and $(T_R)_{calc}/T_w$ is computed from the polynomials by substituting $N_1 i$. There is some advantage in normalizing $(T_R)_{calc}/T_w$ by the value at 300 K, that is, $\left[(T_R)_{calc}/T_w\right]_{300\ K}$, since the normalized ratios are insensitive to small changes in Ni. A polynomial is fitted through

the normalized temperature ratios as a function of temperature and stored on the computer for use in successive iterative steps. If $R(T)$ denotes the normalized temperatur ratio at temperature T_w, then $\left[\left(T_R\right)_{calc}/T_w\right]_{T_1} = R(T_1)\left[\left(T_R\right)_{calc}/T_w\right]_{300\ K}$ is obtained by substituting T_1 and $N_1 i$ into the relevant polynomials. A better estimate of the temperature is $T_R = \left(T_R\right)_{calc}\Big/\left[\left(T_R\right)_{calc}/T_w\right]_{T_1}$. With N_1 fixed, the loop is repeated by substituting this improved estimate into the polynomials until the calculated temperature converges to a constant value T_2. A second estimate of the density N_2 can then be obtained by using T_2 and the quenching cross sections given in reference 8. Repeating this process gives successive estimates of temperature and density. If the estimate N_1 was reasonable, the original polynomial for $R(T)$ can be used for each iterative step without making serious errors. This procedure involves more computation than that given previously (ref. 8) but allows a greater range of Ni to be covered at low temperatures.

Other correction procedures were investigated and one consequence of the proposed secondary-electron excitation model is that $\sum_{K'} \Delta I(K')\Big/\left[I_{(0,0)}\right]_{calc} = 0$. This summation varies slowly with the error in the temperature. Combined with large errors in $\Delta I(K')$, this condition makes it impractical to correct the temperatures by minimizing the summation. A simple and apparently successful procedure developed earlier (ref. 10) was based on the incorrect assumption of direct excitation of the $N_2^+ B^2\Sigma$ states by secondary electrons. Subsequent study shows that the equations in reference 10 are approximate functions fitted through Ashkenas' data. (See ref. 6.) The successful application of this procedure in reference 21 is the result of similar beam currents and geometry for the two experiments. Correcting this shock-layer data (ref. 21) by the present method did not change the temperatures sufficiently to affect the conclusions of that paper.

CONCLUDING REMARKS

Rotational temperatures measured by the electron-beam fluorescence technique increase with density and beam current and depend on which spectral lines are used. The secondary mechanism responsible for the high rotational temperatures cannot be conclusively identified, but excitation of the ground-state rotational levels by low-energy secondary electrons can account for all the observed results. This excitation mechanism redistributes the molecules among the ground-state rotational levels and thus increases the population of the sparsely populated levels at the expense of the more abundantly populated levels.

For this excitation model, the spatial distribution and number density of the secondary electrons and the field of view of the optical system determine the rotational-temperature error for a given density. High flow velocities can influence the measurements through collisions with ions, and thus result in a different spatial distribution of electrons and ions around the beam. For low densities, when the secondary-electron mean free path is large compared with the beam diameter or field-of-view width, there is little influence of high flow velocities. At high densities, when the secondary-electron mean free path is relatively small, the calculated temperature is insensitive to the secondary-electron number density, and hence to all but strong effects of the flow on the distribution of the secondary electrons in the observed gas volume. For these two regimes the present correction scheme should be reliable, but at intermediate densities the flow will reduce the secondary electron concentration in the observed gas volume and the temperature will be underestimated.

Further studies are needed to establish reliable correlating parameters for the calculated temperatures and to determine more accurately the effect of high flow velocities, particularly at intermediate densities.

Langley Research Center,
National Aeronautics and Space Administration,
Hampton, Va., October 26, 1971.

REFERENCES

1. Lillicrap, D. C.; and Berry, C. J.: Experimental Model for High-Speed Rarefied Flow Over a Sharp Flat Plate. Phys. Fluids, vol. 13, no. 5, May 1970, pp. 1146-1152.

2. Fischer, Michael C.; Maddalon, Dal V.; Weinstein, Leonard M.; and Wagner, Richard D., Jr.: Boundary Layer Surveys on a Nozzle Wall at M = 20 Including Hot-Wire Fluctuation Measurements. AIAA Paper No. 70-746, 1970.

3. Beckwith, Ivan E.; Harvey, William D.; and Clark, Frank L. (With appendix A by Ivan E. Beckwith, William D. Harvey, and Christine M. Darden and appendix B by William D. Harvey, Lemuel E. Forrest, and Frank L. Clark): Comparisons of Turbulent-Boundary-Layer Measurements at Mach Number 19.5 With Theory and an Assessment of Probe Errors. NASA TN D-6192, 1971.

4. Wallace, J. E.: Hypersonic Turbulent Boundary-Layer Measurements Using an Electron Beam. Compressible Turbulent Boundary Layers, NASA SP-216, 1968, pp. 255-308.

5. Muntz, E. P.: The Electron Beam Fluorescence Technique. AGARDograph 132, Dec. 1968.

6. Ashkenas, Harry: Rotational Temperature Measurements in Electron-Beam Excited Nitrogen. Phys. Fluids, vol. 10, no. 12, Dec. 1967, pp. 2509-2520.

7. Maguire, Bernadette L.: Density Effects on Rotational Temperature Measurements in Nitrogen Using the Electron Beam Excitation Technique. Rarefied Gas Dynamics, Vol. II, Leon Trilling and Harold Y. Wachman, eds., Academic Press, Inc., 1969, pp. 1761-1782.

8. Lillicrap, D. C.: Experimental Determination of Density and Rotational Temperature by an Improved Electron Beam Technique. AIAA Paper No. 71-605, June 1971.

9. Robben, F.; and Talbot, L.: Measurements of Rotational Temperatures in a Low Density Wind Tunnel. Phys. Fluids, vol. 9, no. 4, Apr. 1966, pp. 644-652.

10. Lillicrap, D. C.; and Harvey, J. K.: Electron-Beam Rotational Temperature Measurements Including the Effect of Secondary Electrons. AIAA J., vol. 7, no. 5, May 1969, pp. 980-982.

11. Smith, Ronald B.: N_2 First Negative Band Broadening Due to Electron Beam Excitation. Rarefied Gas Dynamics, Vol. II, Leon Trilling and Harold Y. Wachman, eds., Academic Press, Inc., 1969, pp. 1749-1760.

12. Hickman, Roy Scott: Rotational Temperature Measurements in Nitrogen Using an Electron Beam. AFOSR 66-2509, U.S. Air Force, Sept. 1966. (Available from DDC as AD 645 113.)

13. Bienkowski, G. K.; and Harbour, P. J.: Structure of Electron-Beam Generated Plasma. Rarefied Gas Dynamics, Vol. II, Leon Trilling and Harold Y. Wachman, eds., Academic Press, Inc., 1969, pp. 1651-1658.

14. Self, S. A.; and Ewald, H. N.: Static Theory of a Discharge Column at Intermediate Pressures. Phys. Fluids, vol. 9, no. 12, Dec. 1966, pp. 2486-2492.

15. Harbour, P. J.; Bienkowski, G. K.; and Smith, R. B.: Influence of Secondary Electrons on an Electron-Beam Probe. Phys. Fluids, vol. 11, no. 4, Apr. 1968, pp. 800-803.

16. Takayanagi, Kazuo; and Takahashi, Tan: Behavior of Slow Electrons in Atmospheric Gases. Part III – Collision Cross Section of Molecular Nitrogen. Report of Ionosphere and Space Research in Japan, vol. 20, no. 4, Dec. 1966, pp. 357-373.

17. Dunn, D. A.; and Self, S. A.: Static Theory of Density and Potential Distribution in a Beam-Generated Plasma. J. Appl. Phys., vol. 35, no. 1, Jan. 1964, pp. 113-122.

18. Williams, William D.: Laboratory Verification Studies of Rotational and Vibrational Temperature Measurements by the Electron Beam Technique. AEDC-TR-68-265, U.S. Air Force, Feb. 1969. (Available from DDC as AD 683 001.)

19. Petrie, S. L.; and Boiarski, A. A.: The Electron Beam Diagnostic Technique for Rarefied Flows at Low Static Temperatures. Rarefied Gas Dynamics, Vol. III, Leon Trilling and Harold Y. Wachman, eds., Academic Press, Inc., 1969, pp. 1685-1701.

20. Hunter, William W., Jr.: Investigation of Temperature Measurements in 300° to 1100° K Low-Density Air Using an Electron Beam Probe. NASA TN 4500, 1968.

21. Lillicrap, D. C.; and Berry, C. J.: Rotational Temperature Measurements in Low-Density Flows. AIAA J., vol. 8, no. 11, Nov. 1970, pp. 2078-2080.

22. Williams, W. D.; Hornkohl, J. O.; and Lewis, J. W. L.: Electron Beam Probe for a Low Density Hypersonic Wind Tunnel. AEDC TR-71-61, U.S. Air Force, July 1971.

NASA-Langley, 1971 — 12 L-8011

"The aeronautical and space activities of the United States shall be conducted so as to contribute . . . to the expansion of human knowledge of phenomena in the atmosphere and space. The Administration shall provide for the widest practicable and appropriate dissemination of information concerning its activities and the results thereof."

— NATIONAL AERONAUTICS AND SPACE ACT OF 1958

NASA SCIENTIFIC AND TECHNICAL PUBLICATIONS

TECHNICAL REPORTS: Scientific and technical information considered important, complete, and a lasting contribution to existing knowledge.

TECHNICAL NOTES: Information less broad in scope but nevertheless of importance as a contribution to existing knowledge.

TECHNICAL MEMORANDUMS: Information receiving limited distribution because of preliminary data, security classification, or other reasons.

CONTRACTOR REPORTS: Scientific and technical information generated under a NASA contract or grant and considered an important contribution to existing knowledge.

TECHNICAL TRANSLATIONS: Information published in a foreign language considered to merit NASA distribution in English.

SPECIAL PUBLICATIONS: Information derived from or of value to NASA activities. Publications include conference proceedings, monographs, data compilations, handbooks, sourcebooks, and special bibliographies.

TECHNOLOGY UTILIZATION PUBLICATIONS: Information on technology used by NASA that may be of particular interest in commercial and other non-aerospace applications. Publications include Tech Briefs, Technology Utilization Reports and Technology Surveys.

Details on the availability of these publications may be obtained from:

SCIENTIFIC AND TECHNICAL INFORMATION OFFICE

NATIONAL AERONAUTICS AND SPACE ADMINISTRATION

Washington, D.C. 20546